Various synchronous states due to coupling strength inhomogeneity and coupling functions in systems of coupled identical oscillators

Cite as: Chaos **29**, 011106 (2019); doi: 10.1063/1.5083621
Submitted: 29 November 2018 · Accepted: 3 January 2019 ·
Published Online: 23 January 2019

Junhyeok Kim,[1,a)] Joon-Young Moon,[2,a)] Uncheol Lee,[3] Seunghwan Kim,[1] and Tae-Wook Ko[4,b)]

AFFILIATIONS

[1]Nonlinear and Complex Systems Laboratory, Department of Physics, Pohang University of Science and Technology, Pohang 37673, Republic of Korea
[2]Department of Psychological and Brain Sciences, Johns Hopkins University, Baltimore, Maryland 21209, USA
[3]Center for Consciousness Science, Department of Anesthesiology, University of Michigan Medical School, Ann Arbor, Michigan 48109, USA
[4]National Institute for Mathematical Sciences, Daejeon 34047, Republic of Korea

[a)]**Contributions:** J. Kim and J.-Y. Moon contributed equally to this work.
[b)]**Author to whom correspondence should be addressed:** twko@nims.re.kr

ABSTRACT

We study the effects of coupling strength inhomogeneity and coupling functions on locking behaviors of coupled identical oscillators, some of which are relatively weakly coupled to others while some are relatively strongly coupled. Through the stability analysis and numerical simulations, we show that several categories of fully locked or partially locked states can emerge and obtain the conditions for these categories. In this system with coupling strength inhomogeneity, locked and drifting subpopulations are determined by the coupling strength distribution and the shape of the coupling functions. Even the strongly coupled oscillators can drift while weakly coupled oscillators can be locked. The simulation results with Gaussian and power-law distributions for coupling strengths are compared and discussed.

Coupled oscillator systems have been widely used as models for systems of interacting elements such as flashing fireflies, chemical oscillators, and neural networks. The systems can show various synchronous behaviors such as in-phase synchronization, full locking, and partial locking. The inhomogeneity in the intrinsic frequencies of the elements has been considered as the main factor that makes the systems desynchronize and causes imperfect synchronous states such as full locking and partial locking. Here, motivated by the recent findings on a wide range of the connectivity level in complex systems such as world-wide web (WWW) and the brain, we focus on the effects of another type of inhomogeneity: inhomogeneity in how strongly individual oscillators are coupled to others on average. We show that this inhomogeneity in the coupling strength combined with the coupling function, which represents the interaction between oscillators, can induce various synchronous states including partial locking in the system of identical oscillators. These various states are categorized, and condition for each category is obtained through the stability analysis.

I. INTRODUCTION

Systems of coupled oscillators have been widely studied as models for a variety of systems in physics, chemistry, and biology.[1–6] The main factors that affect the dynamics of the coupled oscillators are the intrinsic dynamics of oscillators,[1–6] the couplings between oscillators,[6–8] and the connectivity among oscillators.[7,9,10] The recent finding that the connection topology and coupling strength of the networks of systems such as the world-wide web (WWW), the Internet, social and biological networks can be far from being homogeneous[11–13] has spurred interests in the relationship

between the connectivity and the dynamics of systems.[9,10] Previous studies showed that the inhomogeneity in the connectivity distribution or the strength distribution can induce asynchronous states or hinder synchronization.[14–21]

Especially, Ko and Ermentrout showed that inhomogeneity in coupling strength, i.e., inhomogeneity in how strongly single oscillators are coupled to other oscillators on average, makes partially locked states possible even in systems of coupled identical phase oscillators.[20] They studied the special cases with the power-law distributed coupling strength and the coupling function reduced from diffusive coupling. It was shown that the systems can exhibit partially locked states with weakly coupled oscillators locked and strongly coupled ones drifting. In contrast, it was shown in the study by Moon *et al.* that phase-shifted sinusoidal coupling function may induce partially locked states with strongly coupled oscillators locked instead.[21] These contrasting results seem to imply that the coupling strength inhomogeneity and different types of coupling functions can cause various types of partially locked states and possibly other types of synchronous states, but this case has not been clearly investigated.

In this paper, we study the effects of inhomogeneity in coupling strengths and the shapes of coupling functions on the locking behaviors of systems of coupled identical oscillators. It is shown that these two factors together can produce a rich repertoire of synchronous behaviors. We analytically find the conditions for different categories of fully locked or partially locked states. Numerical simulations with Gaussian and the power-law distributions for the coupling strengths confirm our findings.

II. MODEL AND ANALYSIS

Here, we consider the following mean-field model for a phase-reduced system of weakly coupled identical limit cycle oscillators with (in)homogeneous coupling strengths.[19,20]

$$\dot{\theta}_i = \omega + \frac{K_i}{N}\sum_{j=1}^{N}[c_0 + \sin(\theta_j - \theta_i - \beta)],$$
$$i = 1, 2, \ldots, N, \quad c_0 \geq 0, \quad \beta \in [0, \pi/2), \tag{1}$$

where $\theta_i(t)$ is the phase of an oscillator i at time t, ω is the intrinsic frequency of the oscillators, and N is the total number of oscillators. The second term on the right hand side comes from the coupling of oscillators. $K_i(>0)$ is the effective coupling strength to an oscillator i from others. The coupling function $H(\theta) = c_0 + \sin(\theta - \beta)$ is a first order approximation for many general coupling functions obtained from the phase reduction method.[3–6] The coefficient of the second term of H is set to 1 without a loss of generality. The constants c_0 and β determine the shape of the coupling function H. Time delays in interactions can additionally increase the value of β.[22] The constant c_0 is typically less than 1, but for better understanding of the phase diagram we also consider $c_0 \geq 1$.

We investigate the effects of c_0, β, and $\{K_i\}$ on the dynamics of coupled oscillators. Note that the system shows in-phase synchronous states only with either $c_0 = \sin\beta$ or the K_i being the same for all oscillators. We are interested in the systems with inhomogeneous values of K_i. Previous studies with $c_0 = \sin\beta$[20] and $c_0 = 0$[21] show the occurrence of partially locked states with locking of weakly coupled oscillators (defined as the oscillators with small values of K_i) and strongly coupled oscillators (defined as the oscillators with large values of K_i), respectively.

To find out the effect of c_0, β, and $\{K_i\}$ on the dynamical states of the system, we perform a self-consistency analysis as in Ref. 20 for this mean-field model in a more general setting.

Let Ω denote the frequency of the population oscillation described by the order parameter $Re^{i\Theta} \equiv \frac{1}{N}\sum_{j=1}^{N} e^{i\theta_j}$ in a stationary state. Then

$$\dot{\phi}_i = \Delta + K_i[c_0 + R\sin(\Phi - \phi_i - \beta)], \tag{2}$$

where $\phi_i \equiv \theta_i - \Omega t$, $\Delta \equiv \omega - \Omega$, and $\Phi \equiv \Theta - \Omega t$. When the system reaches a stationary state, R and Φ do not depend on time.

Note that $\Delta + K_i c_0$ acts as a desynchronizing inhomogeneous factor, and $K_i R\sin(\Phi - \phi_i - \beta)$ can act as both a synchronizing inhomogeneous factor and a desynchronizing inhomogeneous factor. The coupling strength K_i is involved in both of the competing factors. Thus, it is not intuitively obvious which subpopulation of oscillators will be locked. Note that even when $c_0 = 0$, the system can have partially locked states as shown below.

The oscillators phase-locked with a frequency Ω in the original frame are those with $K_i \in \mathcal{D}_l \equiv \{K_i : K_i R > |\Delta + K_i c_0|\}$ asymptotically approaching a stable fixed point ϕ_i^* in Eq. (2), satisfying the following equations:

$$\Delta + K_i c_0 = K_i R\sin(\phi_i^* - \Phi + \beta) \tag{3}$$

from $\dot{\phi}_i = 0$, and

$$\cos(\phi_i^* - \Phi + \beta) > 0 \tag{4}$$

for the stability of the fixed point.

From Eqs. (3) and (4), we obtain the fixed points

$$\phi_i^* = \sin^{-1}\left[\frac{\Delta + K_i c_0}{K_i R}\right] + \Phi - \beta. \tag{5}$$

The value of ϕ_i^* for each K_i can give useful information for further analysis. The slope of (K_i, ϕ_i^*) curve for locked oscillators can describe the phase distribution over the oscillators with regard to the distribution of the coupling strength. The slope is given by

$$\frac{\partial\phi_i^*}{\partial K_i} = -\frac{\Delta}{{K_i}^2 R\cos(\phi_i^* - \Phi + \beta)}. \tag{6}$$

With the condition in Eq. (4), the sign of the slope reduces to

$$\mathrm{sign}\left(\frac{\partial\phi_i^*}{\partial K_i}\right) = -\mathrm{sign}(\Delta). \tag{7}$$

This means only the sign of Δ determines the sign of the slope, and the phase monotonically increases or decreases as the K_i increases in the locking range of K_i. When the locked oscillators oscillate with a frequency Ω greater than the intrinsic frequency ω ($\Delta < 0$), the slope is positive.

TABLE I. Categorization of the synchronous states: the name of the state is given as Sn_x: n is the major category index and x is composed of d, l^+, l^-, and l^0, where d stands for a drifting range of K, l for a locking range of K, l^+, l^-, l^0, respectively, for positive slope, negative slope, and zero slope of the curve (K_i, ϕ_i^*) in the locking range of K. $\Delta \equiv \omega - \Omega$. For the details, see the text.

States	Oscillators with K from K_{min} to K_{max}	Slope of (K_i, ϕ_i^*)	Sign(Δ)	(R, c_0)	Locking range of K	Additional condition
$S1_{l^0}$	In-phase synchronous	0	0	$R > c_0$	$[K_{min}, K_{max}]$	$R = 1$
$S1_{dl^+}$	Drifting–locked	+	−	$R \geq c_0$	$\frac{\lvert\Delta\rvert}{R+c_0} < K_i$	$K_{min} \leq \frac{\lvert\Delta\rvert}{R+c_0}$
$S1_{l^+}$	Fully locked	+	−	$R \geq c_0$	$[K_{min}, K_{max}]$	$\frac{\lvert\Delta\rvert}{R+c_0} < K_{min}$
$S2_{dl^-}$	Drifting–locked	−	+	$R > c_0$	$\frac{\Delta}{R-c_0} < K_i$	$K_{min} \leq \frac{\Delta}{R-c_0}$
$S2_{l^-}$	Fully locked	−	+	$R > c_0$	$[K_{min}, K_{max}]$	$\frac{\Delta}{R-c_0} < K_{min}$
$S3_{dl^+d}$	Drifting–locked–drifting	+	−	$R < c_0$	$\frac{\lvert\Delta\rvert}{R+c_0} < K_i < \frac{\lvert\Delta\rvert}{c_0-R}$	$K_{min} \leq \frac{\lvert\Delta\rvert}{R+c_0}, \frac{\lvert\Delta\rvert}{c_0-R} \leq K_{max}$
$S3_{l^+d}$	Locked–drifting	+	−	$R < c_0$	$K_i < \frac{\lvert\Delta\rvert}{c_0-R}$	$\frac{\lvert\Delta\rvert}{R+c_0} < K_{min}, \frac{\lvert\Delta\rvert}{c_0-R} \leq K_{max}$
$S3_{dl^+}$	Drifting–locked	+	−	$R < c_0$	$\frac{\lvert\Delta\rvert}{R+c_0} < K_i$	$K_{min} \leq \frac{\lvert\Delta\rvert}{R+c_0}, K_{max} < \frac{\lvert\Delta\rvert}{c_0-R}$
$S3_{l^+}$	Fully locked	+	−	$R < c_0$	$[K_{min}, K_{max}]$	$\frac{\lvert\Delta\rvert}{R+c_0} < K_{min}, K_{max} < \frac{\lvert\Delta\rvert}{c_0-R}$
$S4_d$	Fully drifting	None	+, 0	$R \leq c_0$	None	...

On the other hand, the oscillators with $K_i \in \mathcal{D}_d \equiv \{K_i : K_i R < |\Delta + K_i c_0|\}$ drift monotonically without locking.

Following similar calculations as in Ref. 20, we can obtain the order parameter contributions from the locked subpopulation and from the drifting subpopulation in the rotating frame. With more general coupling functions, we obtain the following relation:

$$R^2 = ie^{-i\beta}\Bigg[\int_{\mathcal{D}_{tot}} dK\, \frac{g(K)(\Delta + Kc_0)}{K} - i\int_{\mathcal{D}_l} dK\, \frac{g(K)\sqrt{K^2R^2 - (\Delta + Kc_0)^2}}{K} - \int_{\mathcal{D}_d} dK\, \frac{g(K)\mathrm{sign}(Z)\sqrt{(\Delta + Kc_0)^2 - K^2R^2}}{K}\Bigg], \quad (8)$$

where $\mathcal{D}_{tot}$ is the total range of K and $Z(K) \equiv \Delta + Kc_0$. We can numerically solve the above equation for R and Δ for given $g(K)$, c_0, and β.

Now, let us find out the range of K_i with which oscillators are locked and classify the locked states. We can get the range of K_i considering the sign of $\Delta + K_i c_0$, the sign of Δ, and the locking condition $K_i R > |\Delta + K_i c_0|$. The range of K_i and the slope of (K_i, ϕ_i^*) for the locking are as follows:

$$\begin{cases} (a)\ \mathrm{S1}: \dfrac{|\Delta|}{R + c_0} < K_i,\ l^{+(0)} & \text{if } R \geq c_0,\ \Delta \leq 0, \\ (b)\ \mathrm{S2}: \dfrac{\Delta}{R - c_0} < K_i,\ l^- & \text{if } R > c_0,\ \Delta > 0, \\ (c)\ \mathrm{S3}: \dfrac{|\Delta|}{R + c_0} < K_i < \dfrac{|\Delta|}{c_0 - R},\ l^+ & \text{if } R < c_0,\ \Delta < 0, \\ (d)\ \mathrm{S4}: \text{no locking} & \text{if } R \leq c_0,\ \Delta \geq 0, \end{cases} \quad (9)$$

where the two equalities of (a) do not hold at the same time and l^0 is for $\Delta = 0$ in (a). In the above equation, l^-, l^0, and l^+ represent the negative slope of (K_i, ϕ_i^*), the zero, and the positive slope, respectively. Note that if the lower bound for a locking range is less than K_{min} or the upper bound is greater than K_{max}, there exists no drifting range bounding the locking range below or above. Thus, in the cases (a) and (b), there can be two types of states for the system: partially locked states with a locking range bounded below by a drifting range [$S1_{dl^+}$ for (a) and $S2_{dl^-}$ for (b)], and fully locked states [$S1_{l^+}$ for (a) and $S2_{l^-}$ for (b)].

Similarly, with the case (c), the system has 4 different types of states: (1) partially locked states with a locking range in between two drifting ranges ($S3_{dl^+d}$), (2) partially locked states with a locked range bounded above by a drifting range ($S3_{l^+d}$), (3) partially locked states with a locking range bounded below by a drifting range ($S3_{dl^+}$), and (4) fully locked states ($S3_{l^+}$).

The conditions and the characteristics of these states are summarized in Table I.

For the partially locked states $S1_{dl^+}$, $S2_{dl^-}$, and $S3_{dl^+}$, strongly coupled oscillators are locked, while weakly coupled ones drift. This does match our intuition that stronger coupling makes oscillators easier to be locked. In contrast to this, in the state $S3_{l^+d}$, which was first observed in Ref. 20, weakly coupled oscillators are locked while strongly coupled ones drift. The analysis also shows that there exists even such a state $S3_{dl^+d}$ where only the oscillators with intermediate coupling strength are locked. All of these states look similar to those observed in the conventional Kuramoto model with distributed intrinsic frequencies.[3–5] However, in the model with coupling strength inhomogeneity and a given coupling function, the strengths, instead of the intrinsic frequencies of the conventional Kuramoto model, determine whether the subpopulations of oscillators are locked or drift.

III. NUMERICAL SIMULATIONS

A. Cases with Gaussian coupling strength distributions

We numerically simulate the model equation (1) using a fourth order Runge-Kutta method with the intrinsic frequency

$\omega = \pi$, the total number of oscillators $N = 1000$ and the time step $\Delta t = 0.01$.

First, we investigate the case of the Gaussian distribution for the coupling strength distributions. The values for coupling strengths are randomly drawn from a given distribution. For the simplicity of the simulations, randomly selected values from $[0, 2\pi)$ are assigned to the phases of the oscillators as the initial condition. Note that since multistability can occur in this system for some values of the parameters,[19,20] in some regions of the phase diagram where one state is stable, other states (e.g., incoherent states) can be obtained from the simulations.

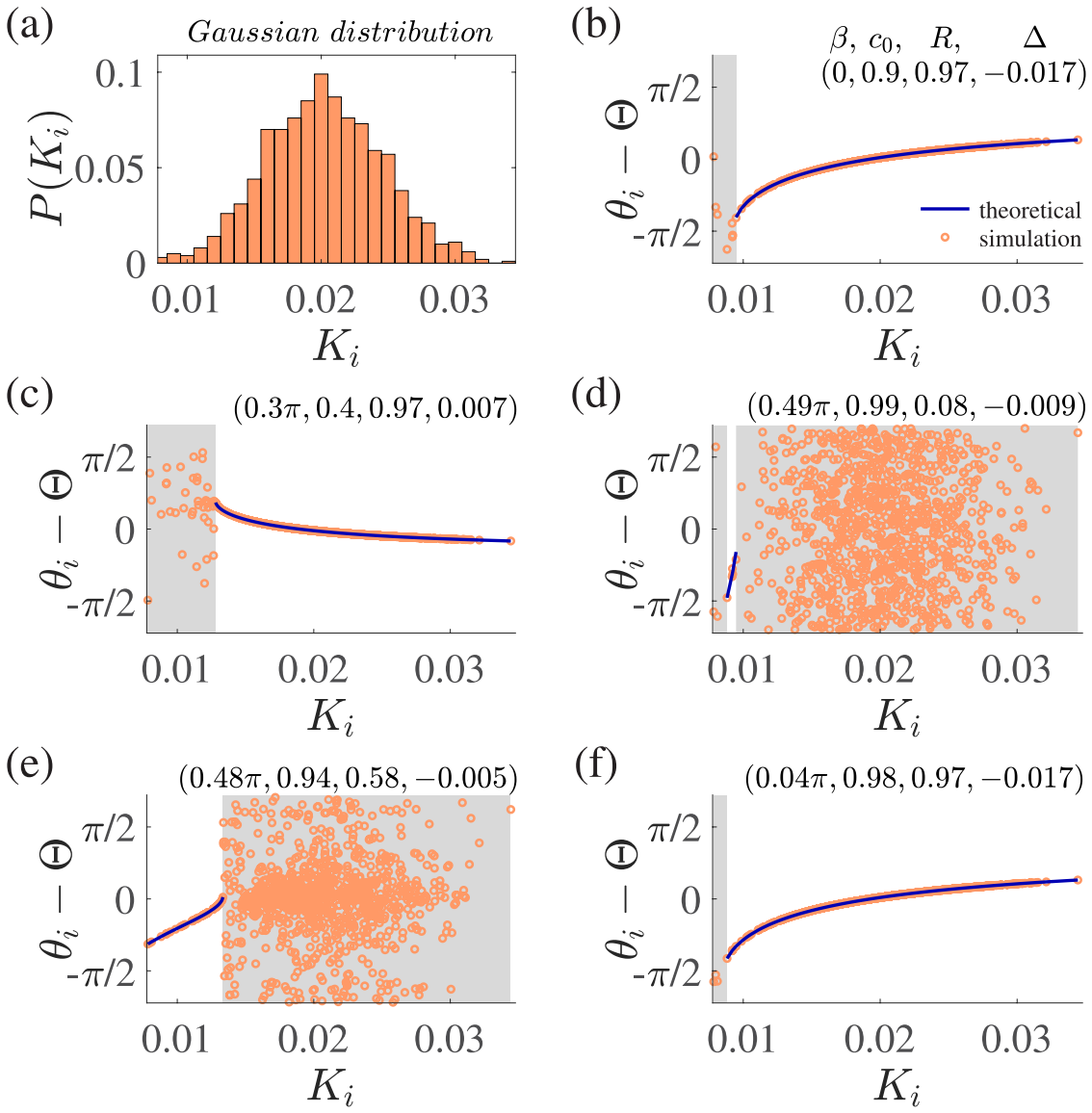

FIG. 1. Gaussian coupling strength distribution and representative partially locked states of the system. (a) Distribution for coupling strengths randomly selected from a Gaussian distribution with a mean of 20×10^{-3} and a standard deviation of 4.5×10^{-3}. For the obtained coupling strength set K_i, $K_{\text{mean}} = 20.2 \times 10^{-3}$, $\sigma_K = 4.36 \times 10^{-3}$, $K_{\text{min}} = 7.85 \times 10^{-3}$, and $K_{\text{max}} = 34.4 \times 10^{-3}$. (b) State $S1_{dl+}$, where d stands for a drifting range of K and l for a locking range: $R > c_0$ and $\Delta < 0$. $K_{\text{min}} < \frac{|\Delta|}{R+c_0} < K_l$, where K_l represents the coupling strength for the locked oscillators. Other details about the state names are as in Eq. (9) and the text below. (c) State $S2_{dl-}$: $R > c_0$ and $\Delta > 0$. $K_{\text{min}} < \frac{\Delta}{R-c_0} < K_l$. (d) State $S3_{dl+d}$: $R < c_0$ and $\Delta < 0$. $K_{\text{min}} < \frac{|\Delta|}{R+c_0} < K_l < \frac{|\Delta|}{c_0-R} < K_{\text{max}}$. (e) State $S3_{l+d}$: $R < c_0$ and $\Delta < 0$. $\frac{|\Delta|}{R+c_0} < K_{\text{min}} \leq K_l < \frac{|\Delta|}{c_0-R} < K_{\text{max}}$. (f) State $S3_{dl+}$: $R < c_0$ and $\Delta < 0$. $K_{\text{min}} < \frac{|\Delta|}{R+c_0} < K_l \leq K_{\text{max}} < \frac{|\Delta|}{c_0-R}$. In (b)–(f), solid lines are theoretical curves for locked phases from Eqs. (5) and (8), and unshaded range is for K_i values for locked subpopulations obtained theoretically from Eq. (9).

The system exhibits in-phase synchronous states with homogeneous coupling strengths or with $c_0 = \sin\beta$. However, with the inhomogeneity in coupling strengths and $c_0 \neq \sin\beta$, the system cannot have in-phase synchronous states, but can exhibit states other states. Note also that the system even with $c_0 = \sin\beta$ can have partially locked states in addition to the in-phase synchronous states in the presence of coupling strength inhomogeneity.[20]

Figure 1 shows the distribution for the coupling strengths [Fig. 1(a)] randomly drawn from a Gaussian distribution and also the partially locked states of the system with the coupling strengths for various combinations of c_0 and β [Figs. 1(b)–1(f)]. In this case, the system has all of the five possible types of partially locked states and the three fully locked states (not shown) as expected theoretically from the conditions as in Eq. (9).

In Figs. 1(b)–1(f), theoretical predictions for (K_i, ϕ_i^*) from Eq. (5) and the values of K_i for the boundaries between locking ranges of K_i fit well with the simulations. The signs of the slopes of (K_i, ϕ_i^*) curve for locking ranges are given by the negative of the sign of Δ as predicted by Eq. (7). Note that while states $S1_{dl+}$ [Fig. 1(b)] and $S2_{dl-}$ [Fig. 1(c)] are similar in that only

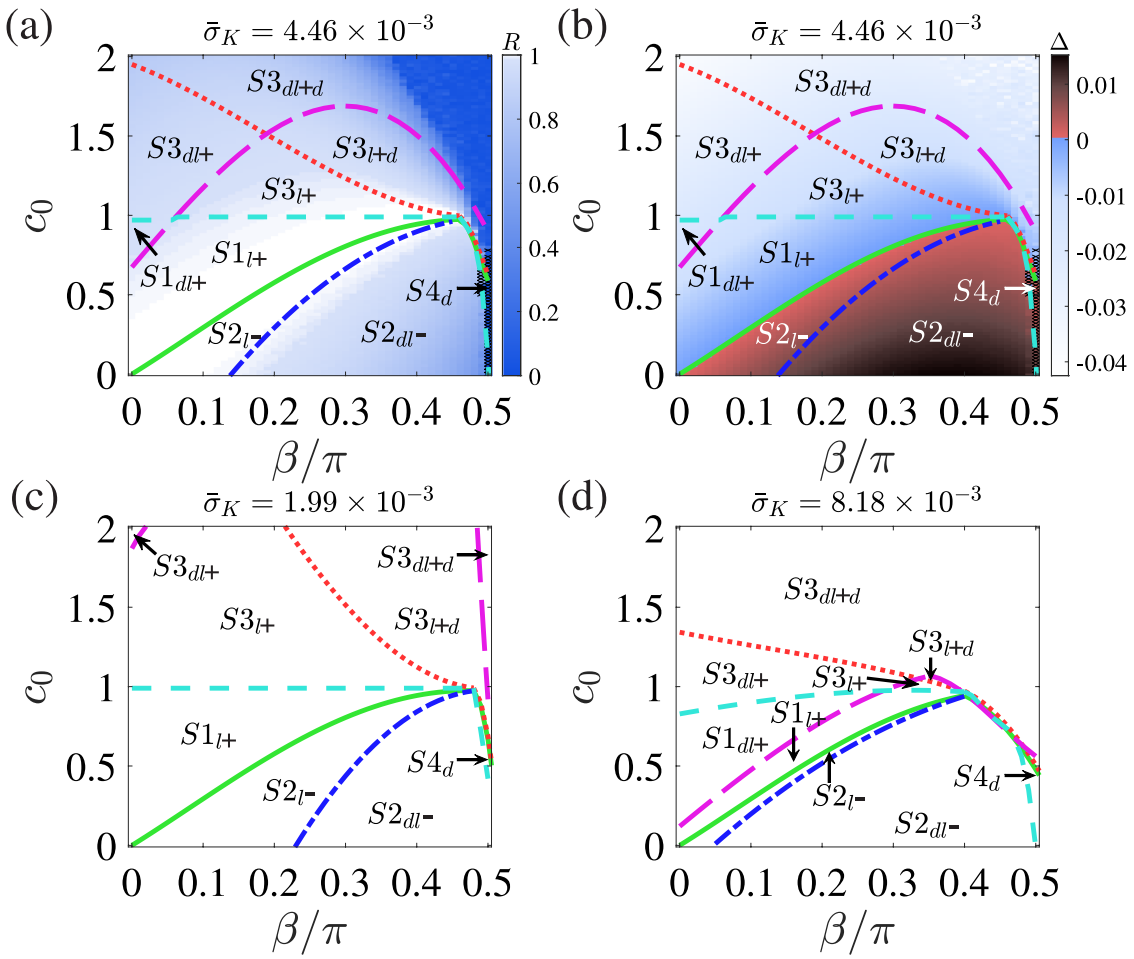

FIG. 2. Phase diagram with the Gaussian coupling strength distribution as a function of c_0 and β determining the shape of coupling function. Phase diagrams (a) with color (gray-scale)-coded order parameter R and (b) with color (gray-scale)-coded $\Delta = \omega - \Omega$. The state names are as in the text. For the simulations, 5 different sets of coupling strengths randomly selected from the same Gaussian distribution ($x_{\text{mean}} = 20 \times 10^{-3}$, $\sigma_x = 4.5 \times 10^{-3}$) are used. The boundaries are determined analytically from Eq. (8) using the conditions [Eq. (9)] for a Gaussian distribution with $(\bar{K}_{\text{mean}}, \bar{\sigma}_K, \bar{K}_{\text{min}}, \bar{K}_{\text{max}}) = (20.1, 4.46, 6.81, 33.91) \times 10^{-3}$, where $\bar{x}$ is the average x of the 5 coupling strength sets. The bounding curves green solid curve, cyan dashed curve, blue dashed-dotted curve, magenta long dashed curve, and red dotted curve are c_0 as a function of β/π obtained for $\Delta = 0$, $R = c_0$, $\frac{\Delta}{R-c_0} = K_{\text{min}}$, $\frac{|\Delta|}{R+c_0} = K_{\text{min}}$, and $\frac{|\Delta|}{c_0-R} = K_{\text{max}}$, respectively. Simulation results match well with the regions. Color (gray-scale)-coded R and Δ are the averaged values from the simulations. The $\times$ symbols near the $\beta = \pi/2$ indicate the occurrence of the incoherent states from the simulations. (c) and (d) phase diagrams with the analytically obtained boundaries for $(\bar{K}_{\text{mean}}, \bar{\sigma}_K, \bar{K}_{\text{min}}, \bar{K}_{\text{max}}) = (20.0, 1.99, 13.9, 26.6) \times 10^{-3}$ and $(\bar{K}_{\text{mean}}, \bar{\sigma}_K, \bar{K}_{\text{min}}, \bar{K}_{\text{max}}) = (20.1, 8.18, 1.12, 39.9) \times 10^{-3}$, respectively. $(x_{\text{mean}}, \sigma_x) = (20, 2) \times 10^{-3}$ for (c) and $(x_{\text{mean}}, \sigma_x) = (20, 9) \times 10^{-3}$ for (d).

strongly coupled oscillators are locked in both of the states, the phases of locked oscillators monotonically increase with increasing K_i in $S1_{dl+}$ and the phases monotonically decrease in $S2_{dl-}$. Strongly coupled oscillators can be phase-leading or phase-lagging depending on the shapes of coupling functions. Note also that in states $S3_{dl+d}$ [Fig. 1(d)] and $S3_{l+d}$ [Fig. 1(e)], strongly coupled oscillators drift while only oscillators with intermediate coupling strengths are locked in $S3_{dl+d}$ and all other oscillators are locked in $S3_{l+d}$.

In Fig. 2, we show the phase diagrams for the system with Gaussian coupling strength distributions. Figures 2(a) and 2(b) are the same phase diagram displayed with color (gray)-coded R and Δ values from the simulations, respectively, for the system with coupling strengths obtained as in Fig. 1. The boundaries between regions for states are determined analytically from Eq. (8) using the conditions in Eq. (9). More details are given in the caption of Fig. 2. Simulation results match well with the corresponding regions. To understand the effects of coupling strength inhomogeneity on the occurrence of the locked and partially locked states, we observe the changes in phase diagrams for coupling strength distributions with standard deviation larger [Fig. 2(c)] and smaller [Fig. 2(d)] than (a).

Let us explain the phase diagrams through the understanding of the boundary curves. The green solid curve for $\Delta = 0$, which has a peak at some value of β (β^*) and is $c_0 = \sin\beta$ for $\beta < \beta^*$, divides the region into two regions with $\Delta < 0$ (states S1, S3) and $\Delta > 0$ (S2, S4), respectively. Equation (3) suggests that the region with $\Delta < 0$ (S1, S3) lies above the $\Delta = 0$ curve. The value R peaks at $R = 1$ on the green solid curve for $\beta < \beta^*$. Another major curve is the cyan dashed curve for $R = c_0$, which lies on or below $c_0 = 1$ and goes through $(c_0, \beta) = (0, 0.5\pi)$ point. This curve divides the region into two regions: one with $R < c_0$ (S3, S4), which lies above the curve, and another with $R > c_0$ (S1, S2).

The curves subdividing the regions are obtained either from the condition (1) that the lower bound of Eq. (9) approaches K_{min} from above or from the condition (2) that the upper bound approaches K_{max} from below. The conditions (1) and (2) result in the shrinking of lower and upper drifting

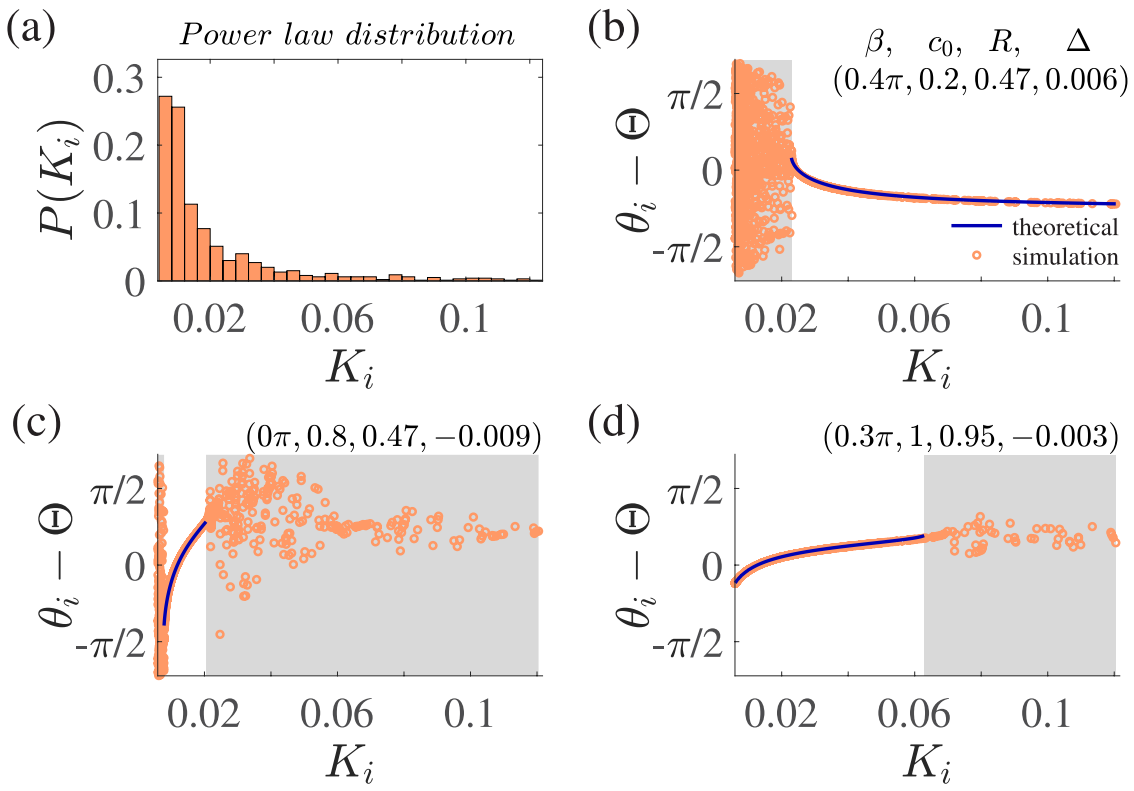

FIG. 3. Power-law coupling strength distribution and representative partially locked states of the system. (a) Distribution for coupling strengths randomly selected from a power-law distribution with a mean of 20×10^{-3} and an exponent of 2. For the obtained coupling strength set K_i, $K_{mean} = 19.9 \times 10^{-3}$, $\sigma_K = 20.5 \times 10^{-3}$, $K_{min} = 6.02 \times 10^{-3}$, and $K_{max} = 120.5 \times 10^{-3}$. (b) State $S2_{dl^-}$, where d stands for a drifting range and l for a locking range. $R > c_0$ and $\Delta > 0$. $K_{min} < \frac{\Delta}{R - c_0} < K_l$, where K_l represents the coupling strength for the locked oscillators. (c) State $S3_{dl^+d}$, $R < c_0$ and $\Delta < 0$. $K_{min} < \frac{|\Delta|}{R + c_0} < K_l < \frac{|\Delta|}{c_0 - R} < K_{max}$. (d) State $S3_{l+d}$, $R < c_0$ and $\Delta < 0$. $\frac{|\Delta|}{R + c_0} < K_{min} \le K_l < \frac{|\Delta|}{c_0 - R} < K_{max}$. Other details are as in Fig. 1.

ranges of K to zero, respectively. The blue dashed-dotted curve, which lies between $S2_{l^-}$ and $S2_{dl^-}$ regions and on the right side of the $S2_{l^-}$ region, is obtained from $\frac{\Delta}{R-c_0} = K_{\min}$. Similarly, the magenta long dashed curve comes from $\frac{|\Delta|}{R+c_0} = K_{\min}$ and acts as boundaries between $S1_{l^+}$ and $S1_{dl^+}$, between $S3_{l^+}$ and $S3_{dl^+}$, and between $S3_{l^+d}$ and $S3_{dl^+d}$. Since the region for $S1_{l^+}$ is located right next to the $\Delta = 0$ curve and $S3_{l^+}$ and $S3_{l^+d}$ can be reachable from $S1_{l^+}$ by changing the parameters without making a lower drifting range of K, all of these states lie below the magenta long dashed curve. With the condition $\frac{|\Delta|}{c_0-R} = K_{\max}$, the red dotted curve separates $S3_{l^+}$ from $S3_{l^+d}$, and $S3_{dl^+}$ from $S3_{dl^+d}$. Regions for $S3_{l^+}$ and $S3_{dl^+}$ lie below the curve.

Summarizing the above, we find that partially locked states emerge away from the green solid curve with high c_0 and/or β near $\pi/2$. In the case of Figs. 2(a) and 2(b), for $c_0 < 1$, which is a probable range for c_0 in the phase-reduction of coupled oscillators, partially locked states $S1_{dl^+}$ and $S2_{dl^-}$ emerge, respectively, at the upper left and the right bottom corners of the rectangle of $0 \le \beta < \pi/2$ and $0 \le c_0 < 1$. In contrast, most of S3 states occur for $c_0 > 1$ except some $S3_{dl^+}$ occurring with c_0 slightly less that 1 and $\beta \approx 0$ and some $S3_{l^+d}$ with large $c_0 < 1$ and $\beta \approx \pi/2$.

With the increase of the standard deviation of the strength distribution, we observe the expansion of the regions for partially locked states for $c_0 < 1$ [Figs. 2(c) → 2(a) → 2(d)].

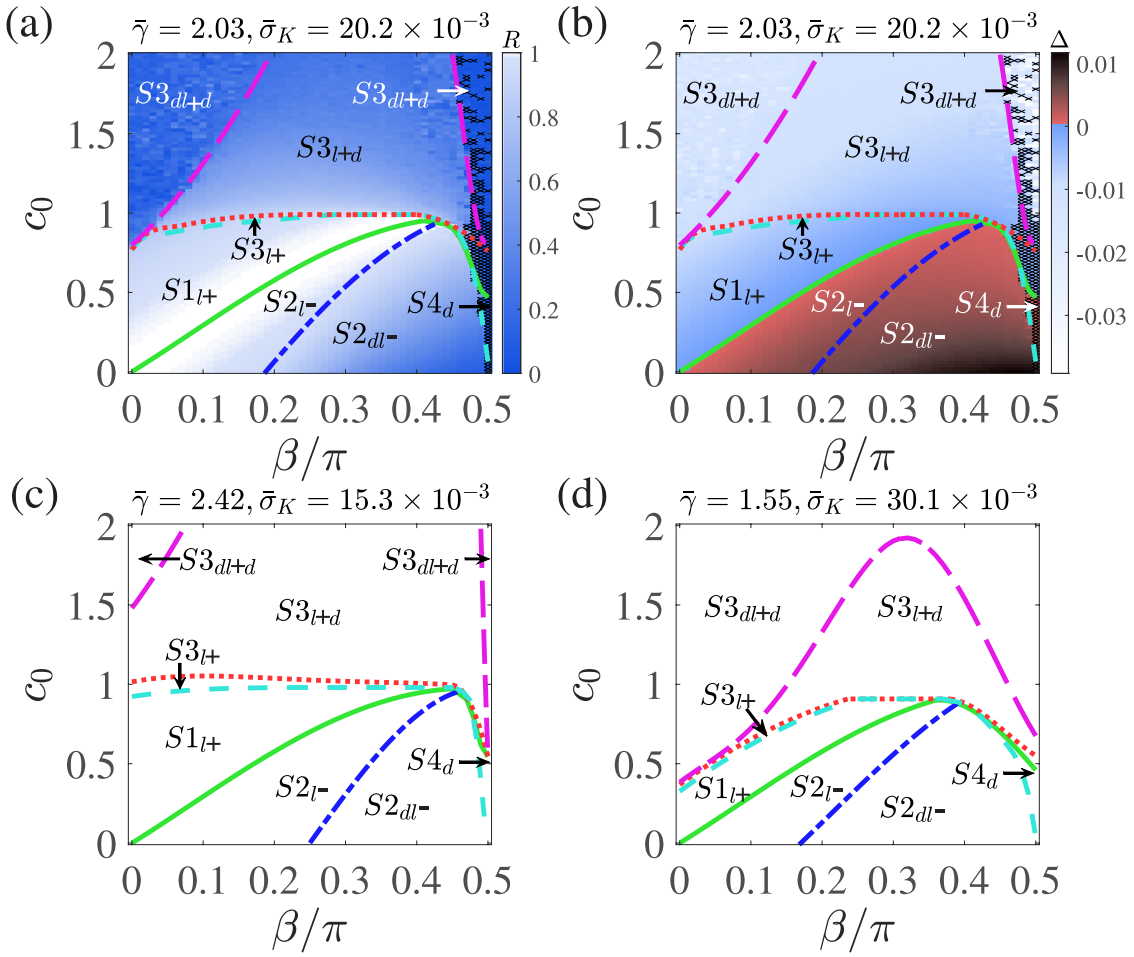

FIG. 4. Phase diagram with power-law coupling strength distribution as a function of c_0 and β. Phase diagrams (a) with color (gray-scale)-coded order parameter R and (b) with color (gray-scale)-coded $\Delta = \omega - \Omega$. The coupling strengths are randomly selected from a power-law distribution $P(x) \sim x^{-\gamma_0}$ with $\gamma_0 = 2$. $\bar{\gamma} = 2.03$, which is the average exponent of distributions for the obtained coupling strength sets, $\bar{K}_{\text{mean}} = 19.8 \times 10^{-3}$, $\bar{\sigma}_K = 20.2 \times 10^{-3}$, $\bar{K}_{\min} = 6.01 \times 10^{-3}$, and $\bar{K}_{\max} = 122.7 \times 10^{-3}$. The boundaries and other details are as in Fig. 2. The $\times$ symbols near the $\beta = \pi/2$ indicate the occurrence of the incoherent states from the simulations. (c) and (d) phase diagrams with the analytically obtained boundaries for $\{\bar{\gamma}, (\bar{K}_{\text{mean}}, \bar{\sigma}_K, \bar{K}_{\min}, \bar{K}_{\max})\} = \{2.42, (20.3, 15.3, 9.00, 97.2) \times 10^{-3}\}$ and $\{1.55, (20.8, 30.1, 2.51, 160.3) \times 10^{-3}\}$, respectively.

Especially, the regions for the states $S3_{dl^+}$ and $S3_{dl^+d}$ expand significantly, and those states become more probable.

B. Cases with power-law coupling strength distributions

Next, we investigate the cases with power-law coupling strength distributions. In Fig. 3(a), we plot the distribution for the coupling strengths randomly drawn from a truncated power-law distribution whose K_{min} and K_{max} are chosen such that the mean value of the distribution matches that of the Gaussian distributions of Figs. 1 and 2. Figures 3(b)–3(d) display the observed partially locked states of the system. In contrast to the Gaussian distribution cases, there are only three types of partially locked states with the power-law coupling strength distributions: $S2_{dl^-}$ [Fig. 3(b)], $S3_{dl^+d}$ [Fig. 3(c)], and $S3_{l^+d}$ [Fig. 3(d)]. Partially locked states $S1_{dl^+}$ and $S3_{dl^+}$ are not observed from the simulations. Figures 4(a) and 4(b) are the corresponding phase diagram with the same parameters. We can notice the absence of the regions for the partially locked states $S1_{dl^+}$ and $S3_{dl^+}$. This absence persists with the decrease [Fig. 4(c)] or increase [Fig. 4(d)] of the standard deviation of the strength distribution with the mean K fixed.

The major differences between the two cases with the different strength distribution are the shrinking of the region between the red dotted curve for $\frac{|\Delta|}{c_0-R} = K_{max}$ and the cyan dashed curve for $R = c_0$, and the merging of the magenta long dashed curve for $\frac{|\Delta|}{R+c_0} = K_{min}$ and the red dotted curve near $\beta = 0$.

With $\frac{|\Delta|}{c_0-R} = K_{max} > 0$, the red dotted curve should be above the cyan dashed curve. In between the two curves, there exists a region for $S3_{l^+}$ states, which satisfy $\frac{|\Delta|}{R+c_0} < K_{min}$ and $\Delta < 0$ from Eq. (9c). For this part of the red dotted curve, we get

$$\frac{K_{max}}{K_{min}} < 1 + \frac{2R}{c_0 - R}. \tag{10}$$

Since $R \in [0,1]$ and K_{max}/K_{min} is very large for large σ_K, c_0 should be close to R. Thus, the part of the red dotted curve bounding above $S3_{l^+}$ is very close to the cyan dashed curve for large σ_K [Figs. 4(a) and 4(d)].

For β close to 0.5π, there are more incoherent states [$\times$ in Figs. 4(a) and 4(b)] than in the cases with Gaussian distributions in numerical simulations due to the strong inhomogeneity of coupling strength.

As the standard deviation of the coupling strength distribution increases, similar to the cases with Gaussian coupling strength distributions, the regions for partially locked states expand in the regions with $c_0 < 1$. Those states $S3_{l^+d}$ and $S3_{dl^+d}$ become significantly more probable [Fig. 4(d)].

IV. CONCLUSIONS

In conclusion, using a mean-field model of coupled oscillators with inhomogeneous coupling strengths, we have studied the effects of the coupling strength inhomogeneity and the coupling functions on the phase locking behaviors of coupled oscillators. Applying a self-consistency argument, we have analyzed the stability of the states of the system and found different types of locked states including partially locked states. Moreover, the condition for various locked states is obtained analytically. The analytic results are in good agreement with the numerical simulations with Gaussian distributions and power-law distributions for coupling strengths.

In a single generalized framework, we have successfully given a unified explanation of the previously observed states[20,21] and shown that the coupling strength inhomogeneity and coupling functions can induce various other states in the absence of inhomogeneity in intrinsic frequencies which has been the focus of studies as the cause of diverse states.[1–5] Chimera states,[7,23] which are spatially extended partially locked states due to spatially nonlocal interactions and coupling functions, seem to be related to the states observed in this study. However, chimera states are different in that the coupling strength inhomogeneity is not a factor for the generation of states.

These results can help to gain a deeper insight into collective dynamics in complex systems, such as the brain, where the connectivity or the coupling strength can be far from being homogeneous.[6,9,13,21,24,25] It will be a very relevant and interesting future study to observe and explain the occurrence of the various states of this present work in real complex systems and the transitions between the states.

ACKNOWLEDGMENTS

This work was partially supported by the National Research Foundation, South Korea (Grant No. 2017R1D1A1B03035456) and partially by the National Institutes of Health (NIH), Bethesda, MD, USA (Grant No. RO1 GM098578). This work was also partially supported by the National Institute for Mathematical Sciences (NIMS) grant funded by the Korea government (MSIT) (No. B18110000).

REFERENCES

[1] A. Pikovsky, M. Rosenblum, and J. Kurths, *Synchronization: A Universal Concept in Nonlinear Sciences* (Cambridge University Press, Cambridge, 2001).
[2] S. H. Strogatz, *Sync: The Emergence Science of Spontaneous Order* (Hyperion Publisher, New York, 2003).
[3] Y. Kuramoto, *Chemical Oscillations, Waves, and Turbulence* (Springer, Berlin, 1984).
[4] S. H. Strogatz, Physica D **143**, 1 (2000).
[5] J. A. Acebrón *et al.*, Rev. Mod. Phys. **77**, 137 (2005).
[6] G. B. Ermentrout and D. Kleinfeld, Neuron **29**, 33 (2001).
[7] M. J. Panaggio and D. M. Abrams, Nonlinearity **28**, R67 (2015).
[8] T. Stankovski, T. Pereira, P. V. E. McClintock, and A. Stefanovska, Rev. Mod. Phys. **89**, 045001 (2017).
[9] A. Arenas, A. Díaz-Guilera, J. Kurths, Y. Moreno, and C. Zhou, Phys. Rep. **469**, 93 (2008).
[10] F. A. Rodrigues, T. K. DM. Peron, P. Ji, and J. Kurths, Phys. Rep. **610**, 1 (2016).
[11] S. H. Strogatz, Nature **410**, 268 (2001).
[12] R. Albert and A.-L. Barabási, Rev. Mod. Phys. **74**, 47 (2002).
[13] O. Sporns, *Networks of the Brain* (MIT Press, Cambridge, 2010).
[14] D. Golomb and D. Hansel, Neural Comput. **12**, 1095 (2000).
[15] M. Denker, M. Timme, M. Diesmann, F. Wolf, and T. Geisel, Phys. Rev. Lett. **92**, 074103 (2004).

[16]T. Nishikawa, A. E. Motter, Y.-C. Lai, and F. C. Hoppensteadt, Phys. Rev. Lett. **91**, 014101 (2003).
[17]A. E. Motter, C. Zhou, and J. Kurths, Europhys. Lett. **69**, 334 (2005); Phys. Rev. E **71**, 016116 (2005).
[18]C. Zhou, A. E. Motter, and J. Kurths, Phys. Rev. Lett. **96**, 034101 (2006).
[19]T.-W. Ko and G. B. Ermentrout, Phys. Rev. E **78**, 026210 (2008).
[20]T.-W. Ko and G. B. Ermentrout, Phys. Rev. E **78**, 016203 (2008).
[21]J.-Y. Moon *et al.*, Sci. Rep. **7**, 46606 (2017).
[22]B. Ermentrout and T.-W. Ko, Phil. Trans. R. Soc. A **367**, 1097 (2009).
[23]N. Zhao, Z. Sun, and W. Xu, Sci. Rep. **8**, 8721 (2018).
[24]F. Varela, J.-P. Lachaux, E. Rodriguez, and J. Martinerie, Nat. Rev. Neurosci. **2**, 229 (2001).
[25]A. Hillebrand *et al.*, Proc. Natl. Acad. Sci. U.S.A. **113**, 3867 (2016).